

# Hydration-Induced Shape and Strength Recovery of the Feather

Tarah N. Sullivan, Yunlan Zhang, Pablo D. Zavattieri, and Marc A. Meyers\*

As necessary appendages to the bird wing for flight, feathers have evolved to address the requirements of aerial locomotion. One of the recently discovered, fascinating aspects of this is their ability to recover shape and strength with hydration. This feature significantly enhances the effectiveness of a bird's flying capability as it allows for the natural restoration of feathers damaged by predators or other external forces. Herein, this capability is analyzed and it is demonstrated that the feather shaft can regain approximately 80% of its strength in the *calamus*, and 70% in the *rachis* when subject to a hydration step after being bent to failure. The matrix of the nano-composite structure within the feather shaft is thought to swell and soften when hydrated, reorienting the stiffer buckled fibers back to their original position. Upon drying, the strength is recovered. Experimental results are found to support this hypothesis, and a finite element calculation of hydration-induced recovery demonstrates the effect. Smart, self-healing composites based on approaches learned from the feather have the potential to allow for the creation of a new class of resilient materials.

## 1. Introduction

Imperative for bird flight, feathers are an evolutionary marvel designed to be lightweight yet able to endure the intense loads of flight.<sup>[1]</sup> Flying feathers of birds consist of a main shaft (*rachis* and *calamus*) and a vane that branches from the *rachis*. The *rachis* is foam filled and rectangular (Figure 1a), while the *calamus* is hollow and elliptical, embedded under the skin (Figure 1b). Although the vane captures the majority of air in flight, it transfers loading to the shaft, which possesses higher rigidity and strength. Integrity of the shaft is therefore essential to a bird's survival, especially since feathers are usually only replaced once a year.<sup>[2]</sup>

Feathers are composed entirely of  $\beta$ -keratin, a "dead tissue" formed by keratinous cells.<sup>[3]</sup> This biopolymer can be considered a hierarchical fiber-reinforced composite (Figure 1c,d): at the subnanoscale crystalline  $\beta$ -keratin filaments ( $\approx 3$  nm in

diameter) are embedded within amorphous matrix proteins. This filament-matrix composite forms macrofibrils ( $\approx 200$  nm in diameter) which are surrounded by amorphous intermacrofibrillar material. Macrofibrils then bundle to form fibers (3–5  $\mu\text{m}$  in diameter) and these in turn form ordered lamellae within the dense exterior of the feather shaft.<sup>[3–7,25]</sup> The fiber direction within these lamellae varies depending on the side and location along the feather shaft<sup>[4]</sup> as well as the species of bird.<sup>[8]</sup>

Studies on  $\alpha$ -keratin reveal that matrix proteins are water sensitive, while intermediate filaments are crystalline and not mechanically affected.<sup>[7,9,10]</sup> Although the structure of  $\beta$ -keratin differs from  $\alpha$ -keratin, both possess a similar structure consisting of an amorphous matrix and crystalline filaments; therefore, the matrix of  $\beta$ -keratin is generally agreed upon as

behaving similarly to that of  $\alpha$ -keratin.<sup>[3,10–12]</sup> Additionally, the mechanical properties of both keratins demonstrate similar sensitivity to water content: as the humidity increases; breaking strain increases, while stiffness and strength decrease.<sup>[3,13]</sup>

Along with other keratinous materials such as animal hair and pangolin scales,<sup>[14–18]</sup> it has been recently demonstrated that the feather has the ability to recover its shape from a deformed state when hydrated.<sup>[11]</sup> The amorphous matrix material in the feather can be likened to a shape memory polymer (SMP). In SMPs, the shape memory effect is often related to changes in the macromolecular structure due to factors, such as glass transition, reversible cross-linking, and melting transition.<sup>[19]</sup> For example, SMPs can be rigid below the glass transition temperature, but rubber-like and deformable above this temperature, allowing the polymer to recover its shape.<sup>[20]</sup> Several investigations of shape memory stimuli of animal hair ( $\alpha$ -keratin) have recently been published by Xiao et al. and indicate that hydration, heat, redox agents, and UV-light can lead to a shape memory response in  $\alpha$ -keratinous materials. Here, hydration is hypothesized to serve as the actuator which raises the  $\beta$ -keratin matrix material above the glass transition point.

In a pioneering study, Liu et al. found that not only the shape of the feather, but also the compressive strength and energy absorption of the feather's internal foam recovers with hydration.<sup>[11]</sup> In this investigation, the foam was cyclically tested in compression to compare hydrated samples with samples that were hydrated and dried before subsequent testing.<sup>[11]</sup> While

Dr. T. N. Sullivan, Prof. M. A. Meyers  
Department of Mechanical and Aerospace Engineering  
University of California  
San Diego, La Jolla, CA 92093, USA  
E-mail: mameyers@eng.ucsd.edu  
Y. Zhang, Prof. P. D. Zavattieri  
Lyles School of Civil Engineering  
Purdue University  
West Lafayette, IN 47907, USA

DOI: 10.1002/adfm.201801250

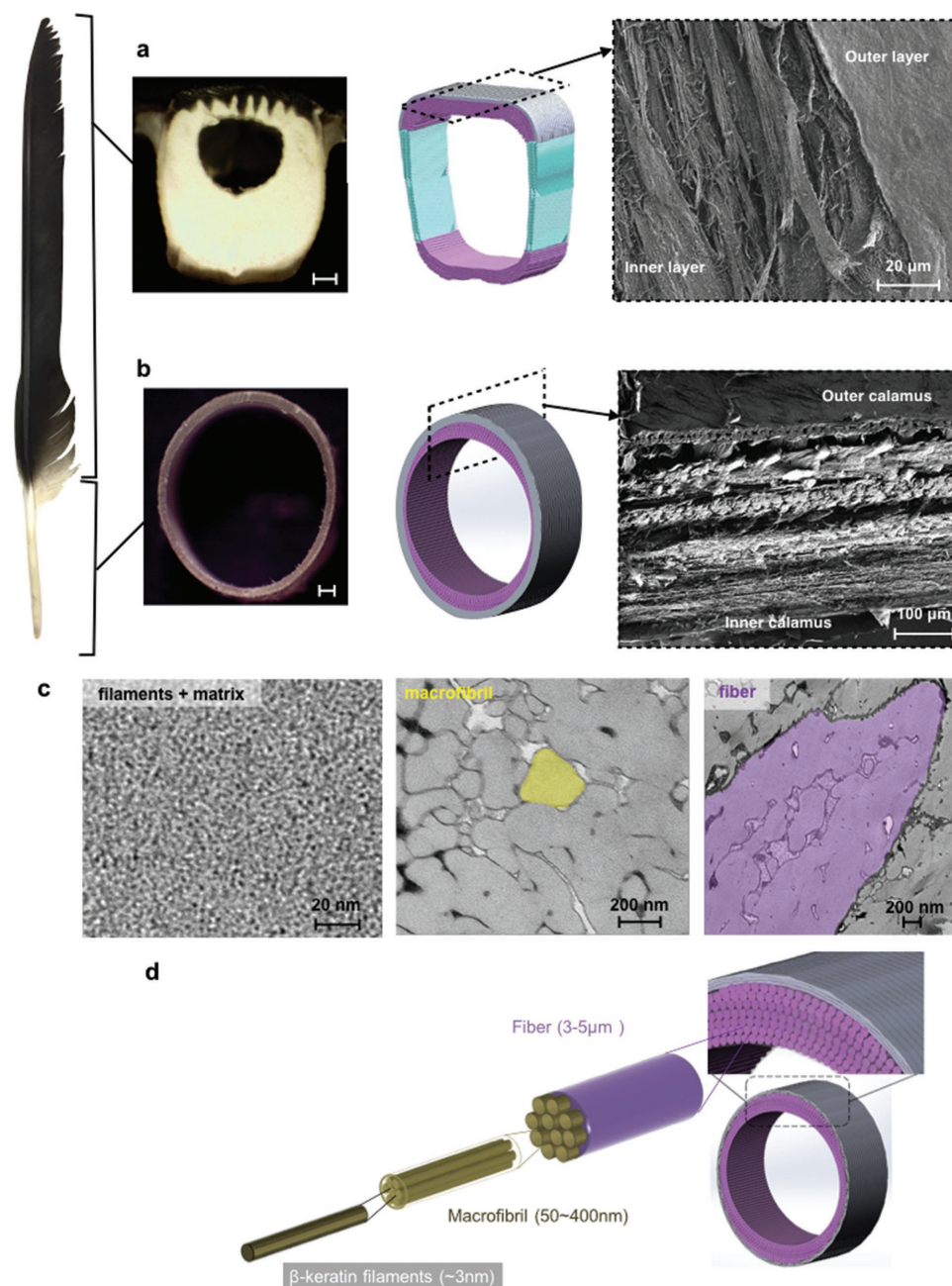


**Figure 1.** The hierarchical structure of the feather: The flight feather of the Cape Vulture (*G. coprotheres*) is divided into the a) *rachis* and b) *calamus*. Optical microscope images of both sections are shown in the leftmost images (scale bar is 0.5 mm). Fiber models of the feather sections illustrate that fibers run longitudinally along the shaft (purple) and circumferentially (gray) within the *calamus* and dorsal side of the *rachis*, while fibers alternate at  $\pm 45^\circ$  angles (green) in the lateral walls of the *rachis*. On the right, scanning electron microscope (SEM) images of the dorsal *rachis* and *calamus* confirm the orientations of fibers in the corresponding sections of fiber models. c) Transmission electron microscope (TEM) images reveal a filament and matrix structure that forms macrofibrils which in turn form fibers, and d) a schematic representation of this is drawn to clarify this structure. Fiber model images in panels (a, b, d) adapted with permission.<sup>[4]</sup> Copyright 2016, the Authors, published by Wiley-VCH.

this research is very significant, in nature the feather is most often subject to flexure and to failure of the entire shaft, not solely the internal foam. Because of this, in our research we conduct cyclical flexure tests on whole sections of the feather shaft. We also compare results between samples with and without a hydration step, which allows the result of a hydration step to be evaluated more effectively.

A model for feather recovery by hydration is proposed and validated through a finite element simulation. This proposed model builds upon Liu et al.'s work by including the swelling of the feather with hydration. However, we state more specifically that the swelling of the matrix and the ensuing straightening of the fibers in the  $\beta$ -keratinous nanocomposite structure are the primary cause of shape and strength recovery. To support this

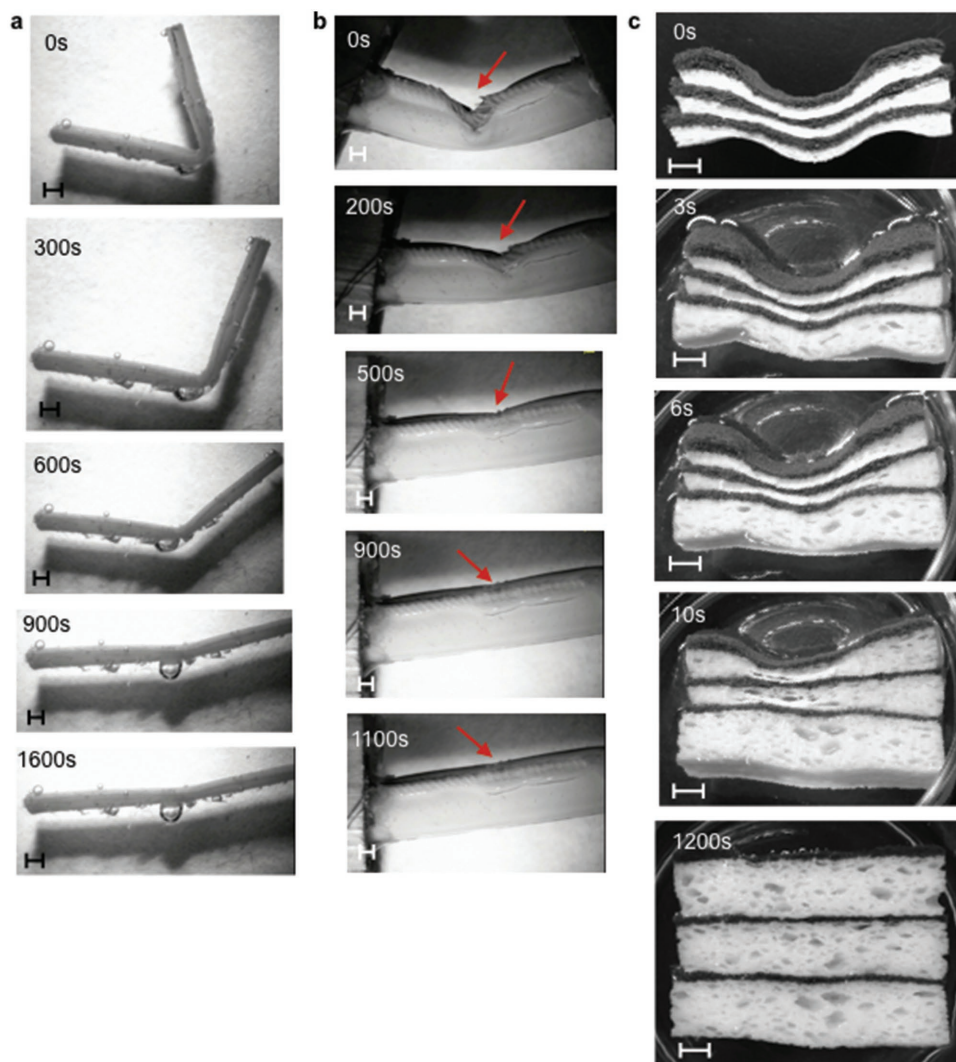


**Figure 2.** Recovery of the feather shaft in water: a) A strip of the feather shaft cortex is severely deformed and recovers in water. b) A *rachis* section with the vane removed is bent and recovers in water; red arrows highlight the location of the deformation. c) The synthetic shape memory composite is shown in its original state, deformed, and hydrated state. The white matrix swells with hydration. Time is indicated in seconds on the top left of each image. Scale bars in panels (a,b) are 1 mm and in panel (c) are 1 cm.

theory, physical measurements of hydrated cortex material are conducted and swelling is found to be largely more apparent in directions perpendicular to fiber length, indicating that it primarily occurs in the matrix material. Research in this area has the potential to lead to the expansion of the capabilities of shape memory composites by incorporating concepts developed by nature over millions of years.

## 2. Results and Discussion

### 2.1. Shape and Strength Recovery of the Feather

Time-lapse images of severely bent cortex and *rachis* sections submerged in water (Figure 2a,b) demonstrate that the feather has the ability to recover its shape when subjected to hydration (this is also presented as a Video S1 in the Supporting Information). While this is quite interesting in itself, evolutionarily it is essential to a bird's

survival for the feather to also recover its strength with hydration. To quantify the feather's strength and bending stiffness recovery, we cyclically tested sections of the *calamus* and *rachis* to failure in four-point bending. Half of the samples tested were hydrated for 24 h after failure and air dried for 72 h before retesting; the other half of samples were left in ambient conditions for 96 h after testing. This allowed both samples to have 96 h of relaxation before subsequent testing. The weight of hydrated samples increased an average of 0.56% (*rachis*) and 0.51% (*calamus*) after 24 h of hydration, and after air drying, dropped back to the original weight of the sample (within  $\pm < 0.1\%$  of original weight).

Results corroborate the strength recovery hypothesis. The effect of shape recovery on strength is demonstrated in the force-displacement plots of five cycles of tests for a *calamus* and *rachis* sample without a hydration step (Figure 3a,c) and with a hydration step (Figure 3b,d); the maximum load corresponds to local buckling. It is clear from these plots that the sample with a hydration step is able to recover its ultimate strength to a

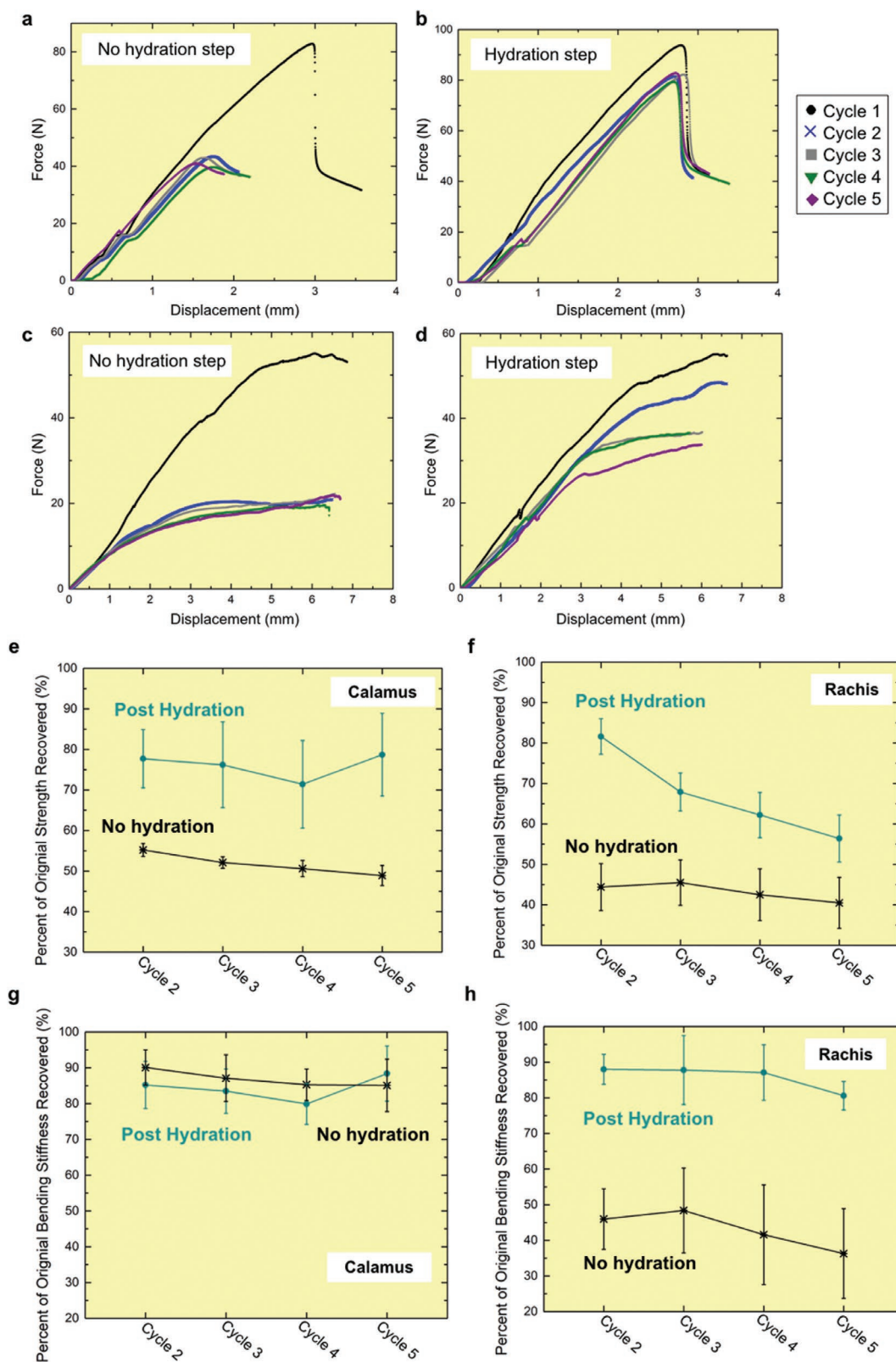


**Figure 3.** Strength recovery and bending stiffness behavior of the feather shaft with a hydration step: Flexural test data of a *calamus* and *rachis* sample a,c) with no hydration step and b,d) with a hydration step between test cycles. The strength recovery of samples, as compared with the maximum strength of cycle one, without a hydration step (black) and with a hydration step (cyan) for e) *calamus* and f) *rachis* samples. The recovered bending stiffness of g) *calamus* and h) *rachis* samples with (cyan) and without (black) a hydration step.

much greater extent than the sample without hydration.

To compare all data of hydrated and non-hydrated samples, the percent difference between the ultimate strength of each cycle and the sample's original cycle (cycle 1) was determined. This value was found for each sample and is called the "percent of original strength recovered." These percentage values are plotted against the cycle number for both the *calamus* (Figure 3e) and the *rachis* (Figure 3f). A general linear model determined that for both the *calamus* and *rachis*, samples with a hydration step have a significantly different percent of strength recovered than the dry samples ( $P = 0.00$ ).

While *rachis* and *calamus* samples with a hydration step recover to a comparable degree during the second cycle ( $81.6 \pm 4.4\%$ ,  $77.7 \pm 7.2\%$ , respectively), *calamus* samples are able to maintain a similar level of recovery throughout the five cycles, while *rachis* samples decrease in recovery to an average of  $56.4 \pm 5.8\%$  by cycle 5. A general linear model confirms this, with significantly different results for recovery between cycle 2 and cycles 3–5 for the *rachis* ( $P = 0.00$ ) and no significant difference between cycles for the *calamus* ( $P > 0.05$ ). Discrepancies in recovery behavior between the *rachis* and *calamus* after the second cycle are due to differences in cross-sectional shape and the presence of foam in the *rachis* sections. As a simpler structure, the *calamus* recovers to a greater extent in later cycles because failure solely occurs on the dorsal side. The *rachis* must recover not only in its dorsal cortex, but also in the lateral walls, which collapse in failure. Additionally, the *rachis*' foam undergoes failure with each cycle, and since it is composed of many very thin fibers, it is subject to unrecoverable damage at the microlevel such as fiber breaking after the second trial. Damage to the *rachis*' internal foam on the fiber level after the initial test cycle was also observed by Liu et al. in compression tests.<sup>[11]</sup>

To examine the degree of internal structural recovery between samples, longitudinal cross sections of hydrated and nonhydrated buckled samples were compared with those of an untested sample. The internal structure of the hydrated sample appeared nearly identical to the untested sample; while the nonhydrated sample demonstrated fiber splitting at the cortex–foam interface and within regions of local buckling (additional information can be found in Section S.1 in the Supporting Information). This microscopic level of recovery allows for not only the shape, but also the strength of feathers to be recovered. After five cycles, the strength of the hydrated *calamus* sample is  $\approx 80\%$  of the original strength, while that of the dry *calamus* is only  $\approx 55\%$ . This strength recovery is important to the flying ability of the bird, after feathers are broken by predator attack, fight, or catastrophic events.

Since feathers are largely optimized for bending stiffness to sustain loading in flight, the average percentage of bending stiffness recovered in cyclical tests of samples with and without a hydration step was plotted (Figure 3g,h). As demonstrated

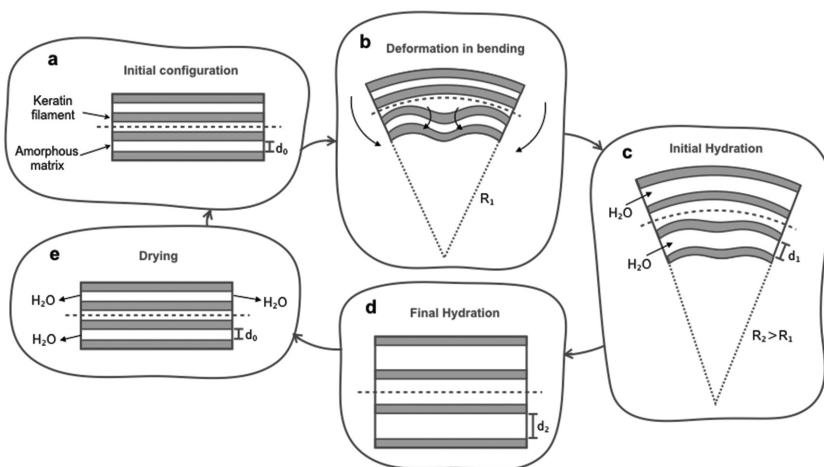


**Figure 4.** The proposed mechanism for shape and strength recovery of the feather shaft. a) The cycle begins in the “initial configuration” showing the composite structure of  $\beta$ -keratin filaments in an amorphous matrix. b) These filaments undergo “deformation in bending” and buckle in compression. c) Hydrated water molecules penetrate preferentially into the amorphous matrix causing swelling (indicated by  $d_1 > d_0$ ) and therefore straightening of filaments as the radius of curvature increases from  $R_1$  to  $R_2$ . d) The matrix then fully swells as spacing grows to  $d_2$  and completely straightens fibers. Last, e) the sample dries and water molecules diffuse out of the amorphous material, which loses its plasticizing effect.

in Figure 3g, the recovered bending stiffness of the *calamus* is comparable with and without a hydration step, while the *rachis* bending stiffness recovers to a much greater extent with a hydration step ( $\approx 86\%$ ) than without one ( $\approx 43\%$ ) (Figure 3g). This is likely due to the reliance of bending stiffness ( $EI$ ) on the area moment of inertia of the sample. The foam within the *rachis* swells with hydration, which allows the original shape of the *rachis* to be recovered. Without hydration the foam remains compressed, therefore altering its cross-sectional shape and lowering its area moment of inertia. Recovery of the shape of the *rachis* is demonstrated in Figure 2b. *calamus* samples, on the other hand, are not affected because their cross-sectional shape does not differ largely between samples with and without a hydration step. Figure S.2 in the Supporting Information shows the side view of the *calamus* for samples with and without a hydration step demonstrating that its overall shape remains comparable independent of the hydration step.

## 2.2. Mechanism for Shape Recovery

A mechanism for the shape and strength recovery of feather keratin is proposed in Figure 4. A feather cortex strip is shown in its initial configuration as a layered  $\beta$ -keratin nanocomposite (Figure 4a). When the feather is bent, buckling occurs with accommodation by the amorphous matrix, which deforms inelastically. This Euler buckling is shown schematically in Figure 4b. As mentioned previously, the matrix is more affected by hydration than the stiffer crystalline fibers.<sup>[3,10–12]</sup> Therefore, upon wetting, water molecules penetrate preferentially into the amorphous matrix, causing it to swell and deform inelastically (Figure 4c). A more detailed drawing of the hydrated response of the matrix is shown in Figure S.3 in the Supporting Information, where water reduces the interchain interaction

and increases the interchain spacing by acting as a cross link between chains.<sup>[12]</sup> The flow stress of the hydrated matrix is assumed to be considerably lower than the fibers. Figure S.4 in the Supporting Information shows the hypothetical response of the cortex during the hydration stage, with the separate responses of the fibers and matrix. Fibers show minimal hydration effect, while the amorphous matrix softens considerably. This is indicated by an increase in spacing between fibers from  $d_0$  to  $d_1$  in Figure 4c. This, in combination with the elastic energy stored in the fibers due to buckling, causes the fibers to straighten, since they are elastically loaded in compression. As a result, the radius of curvature increases from  $R_1$  to  $R_2$ . The matrix swells further in Figure 4d to have a larger spacing  $d_2$  so that fibers completely reorient to their original position. This is accompanied by reverse plastic flow in the matrix that allows the fibers and their surroundings to return to their original geometry. The last stage, dehydration, corresponds to the removal of water molecules from the amorphous matrix, which shrinks back to a spacing  $d_0$  (Figure 4e) without inducing any additional inelastic deformation. Thus, the initial configuration is recreated and the shape recovery cycle is completed. A simplified demonstration of this is shown in Figure 2c, where a bioinspired composite is shown in its original state, deformed, and hydrated. The cellulosic matrix material drives the stiffer dark “fibers” back to their original position when hydrated. Similarities can be drawn between the proposed recovery mechanism of  $\beta$ -keratin and the shape-change of certain plant

tissues, where material anisotropy allows for shape manipulation under stimuli.<sup>[21]</sup>

To determine the correctness of this theory, various dimensions of shaft sections and cortex strips were measured and compared before and after hydration. Significant swelling occurred within samples; **Figure 5b** shows an optical microscopic image of a feather cross section before hydration, with a tracing of the outer surface of the same feather after hydration. Figure 5a plots the percent difference in dimensions of the *calamus* and *rachis* with 24 h of hydration, where measured dimensions of circumference and length are demonstrated in Figure 5c. The *rachis* circumference consistently increases in dimension, while its length does not. The *calamus* shows a less extreme difference in swelling between the length and circumference, with on average less circumferential and more length swelling than the *rachis*.

Figure 5d shows the changes in length, thickness, and width of strips of the dorsal side of the *rachis* and *calamus* (as shown in Figure 5e,f, respectively). The dorsal *rachis* is chosen because it is the side of the *rachis* that undergoes the most damage in flexure and, unlike the *calamus*, each side of the *rachis* has a different fiber orientation. Dorsal *rachis* strips exhibited very low or even negative swelling in the length dimension, with the greatest amount of swelling occurring in the thickness. *calamus* samples, on average, demonstrated less swelling in both thickness and width when compared to the *rachis*, but more swelling in length.

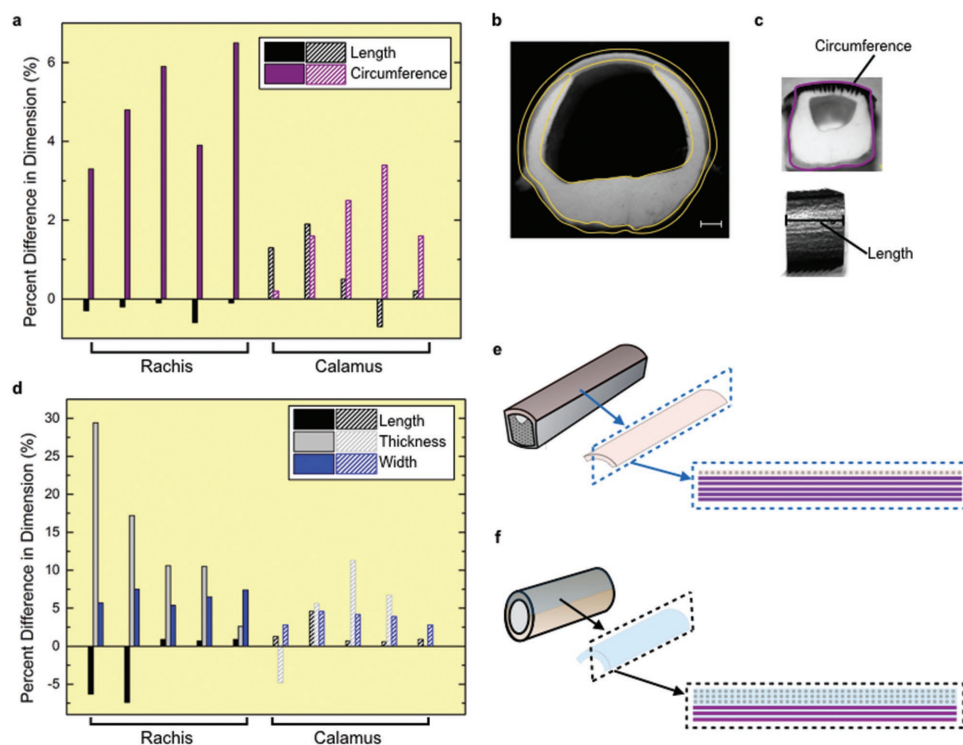


**Figure 5.** The swelling of *rachis* and *calamus* samples with hydration. Experiments were conducted to determine if the feather swells upon hydration: a) the length, circumference and area of cross sections (as shown in panel (c)) of the *rachis* and *calamus* were compared before and after hydration. b) The image shows the initial cross section, while the yellow outline highlights the cross-sectional profile of the sample after hydration (scale bar is 1 mm). d) The length, thickness, and width of cortex strips from the e) dorsal *rachis* and f) *calamus* were measured before and after hydration to determine the percent difference in dimension.

The proposed mechanism described in Figure 4 should theoretically result in hydration-induced swelling in the dimensions perpendicular to the fibers and negligible swelling in the direction of the fibers. While both the dorsal *rachis* and the *calamus* have an inner layer in which fibers run along the length of the shaft and an outer layer in which fibers run perpendicularly to the shaft, the *calamus* has a much thicker outer layer than the *rachis*. This is demonstrated in the scanning electron microscopic images in Figure 1a,b (with further characterization of the *calamus* presented in Figure S.5 in the Supporting Information). As a result, the *calamus* has more fibers running perpendicularly to the shaft than the dorsal *rachis*, as shown in the schematic Figure 5e,f. Based on these differences in fiber alignment, the *rachis* is expected to swell more extremely in thickness and width and less in length than the *calamus*. This hypothesis is supported by the results of the swelling tests, which on average demonstrate this trend. Interestingly, the data indicate that indeed, on average the thickness dimension swells most in the *rachis*. Overall, data show that the feather swells more in the direction perpendicular to the fibers and less in the direction of the fibers. Animal hair ( $\alpha$ -keratin) has also been observed to swell with hydration, with a significant increase in diameter and negligible change in length.<sup>[14,22]</sup>

### 2.3. Simulations of Shape Recovery in the Feather

To verify the hypothesis that the geometry of the feather cortex recovers with hydration, a finite element analysis (FEA) model was developed based on the individual responses of the matrix and fibers. This model attempts to capture the mechanism of the feather cortex hydration recovery process, instead of replicating exactly the same process observed in the experiments. As such, the cortex can be simplified as a representative volume element. This representative volume element, consisting of six fibers embedded in a matrix composite beam (Figure 6a), is created to represent a section of the feather shaft cortex. The FEA model considers plane strain conditions, and the mechanical properties of the fiber and matrix were obtained from hydrated and dehydrated feather cortex properties.<sup>[11]</sup> The fibers were assumed to be unaffected by water content and considered to behave linearly elastically, while the matrix was assumed to be an elastic-perfect plastic material.<sup>[3,10–12]</sup> With an increase in water content, the elastic modulus and yield stress of the matrix decrease and the matrix swells. The analysis was performed in ABAQUS 6.14, and four-node plane strain elements (CPE4R) was used to discretize the model (Figure 6b). More details of the model can be found in the Section S.2 in the Supporting Information. Figure 6c–e shows the loading, hydration, and posthydration process of this cortex section, respectively. The ratio of the absolute maximum in plane principal stress  $\sigma_1$  to the yield stress of the matrix  $\sigma_y$  with zero moisture content was exhibited to indicate the level of plastic deformation of materials during the process. First, a prescribed curvature,  $\kappa_{ap}$ , was applied to the composite by imparting an external bending moment at the ends of the composite. This causes the matrix to plastically deform leading to a permanent curvature,  $\kappa_{pl}$ , shown in Figure 6c. While the composite is plastically deformed, 100% water content was gradually applied to the composite through a

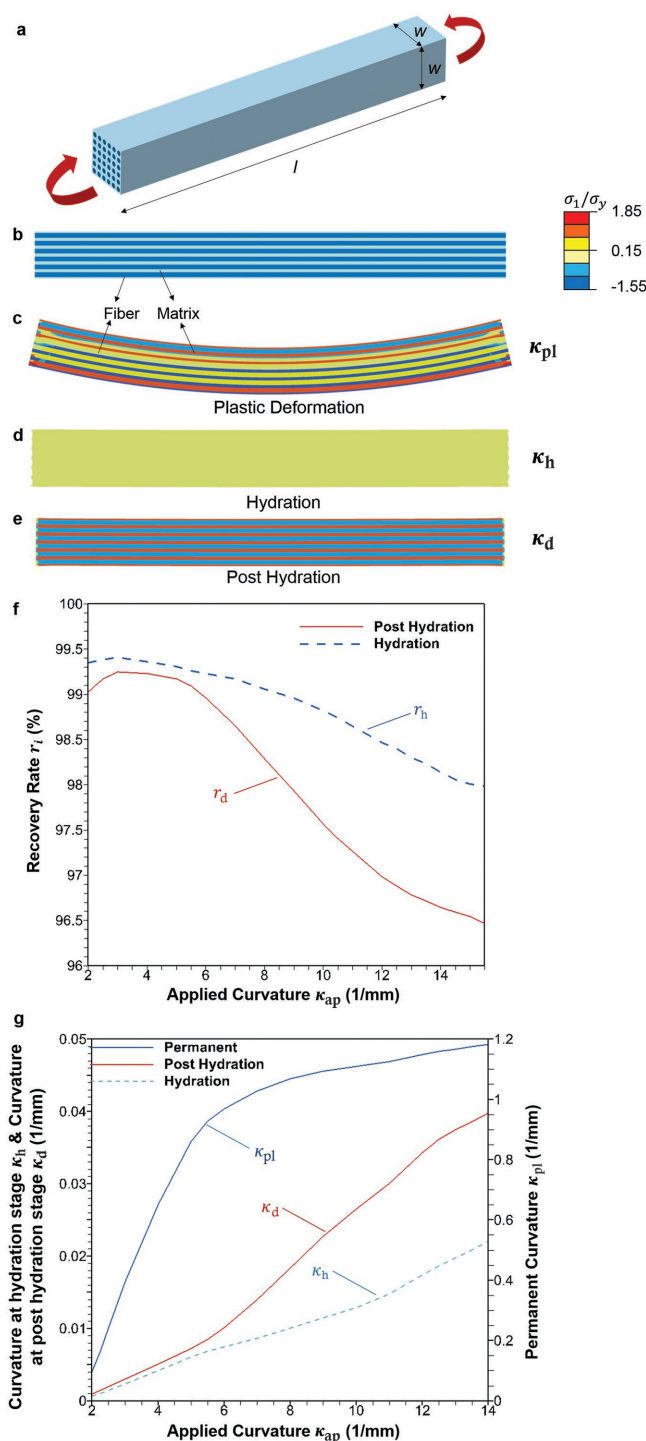


**Figure 6.** Finite element simulations of the shape recovery process. a) Schematic of the representative volume element where an applied curvature is prescribed along the composite to induce plastic deformation in the matrix. b) 2D representation of the plane strain FEA model. c) The deformed composite with residual stress after unloading, where  $\sigma_1$  represents the maximum absolute principal stress,  $\sigma_y = 77.5$  MPa represents the yield stress of matrix when the moisture content is 0. d) After hydration, the residual stress drops significantly and the section regains its shape. e) The composite retains much of this shape recovery post hydration. f) The percent recovery (Equation (1)) after hydration and after posthydration as a function of the applied curvature yields high values of recovery (all above 96%).

hydrostatic strain (Figure 6d). Concomitant with the hydration, the flow stress of the matrix is decreased. The stress in both the fibers and matrix, and therefore the elastic energy stored in the fibers, significantly drops, leading to a much lower curvature,  $\kappa_h$ , of the composite. After complete hydration, a posthydration process was applied to the composite to decrease the water content from 100% to 0% (Figure 6e). This dehydration process leads to a curvature,  $\kappa_d$ , slightly larger than the hydrated curvature.

The shape recovery for the hydration,  $r_h$ , and posthydration,  $r_d$ , steps can be defined by

$$r_i = \left| \frac{\kappa_i - \kappa_{pl}}{\kappa_{pl}} \right| \times 100\% = \left| \frac{\kappa_i}{\kappa_{pl}} - 1 \right| \times 100\% \quad (1)$$

where  $\kappa_i = \kappa_h$  is the curvature of composite beam under 100% hydration, and  $\kappa_i = \kappa_d$  is the curvature of composite at the posthydration stage. Figure 6f shows the shape recovery attained with hydration ( $r_h$ ), and posthydration ( $r_d$ ) as a function of the applied curvature,  $\kappa_{ap}$ . For very low  $\kappa_{ap}$  (up to  $\approx 4 \text{ mm}^{-1}$ ) both  $r_h$  and  $r_d$  increase. However after reaching this peak, both decrease. As the applied curvature increases, material from the top and bottom of the structure starts to experience plastic deformation, while material near the neutral axis undergoes small deformations. The amount of plastic deformation that is accumulated in the matrix competes with the stiffness of the fibers, which ultimately limits the permanent curvature of the structure. Hence, as shown in Figure 6g, applying a larger curvature initially leads to an increase in permanent curvature  $\kappa_{pl}$  but eventually plateaus. It is also shown in Figure 6g, where  $\kappa_h$  and  $\kappa_d$  increase steadily. As a result,  $\frac{\kappa_i}{\kappa_{pl}}$  increases more rapidly after  $\kappa_{pl}$  plateaus, and  $r_i$  exhibits a peak at around 4 ( $1 \text{ mm}^{-1}$ ). While the hydrated sample recovers to a greater extent (99.5%) than the posthydrated sample (96%), both demonstrate a high recovery percentage. This supports the experimental findings of high shape and strength recovery with a hydration step. Ancillary FEA simulations conducted to analyze the effect of any postyield hardening behavior in the matrix (Figure S.7, Supporting Information) showed that the level of hardening had an insignificant influence on the recovery rate (Table S.2, Supporting Information).

### 3. Conclusions

Synergistically, the nanocomposite design and material properties of the feather shaft allow for its shape recovery through a hydration step. Here, we quantitatively prove the feather's ability to recover strength with hydration and explain this phenomenon through experimentally supported models involving the swelling and softening of the feather's matrix material with hydration.

When deformed beyond the buckling limit, both sections of the feather shaft (*calamus* and *rachis*) recover their strength to a considerably greater degree with a hydration step than without one. In cyclical tests, the flexure strength of the *calamus* consistently recovered to a larger extent over multiple cycles ( $\approx 80\%$ ) than the *rachis* ( $\approx 55\%$ ). This is likely due to the macrostructural

differences between the *rachis* and *calamus*, especially the foam within the *rachis* which likely becomes permanently damaged as cycles' progress. Although multiple deformation cycles to the onset of buckling were applied, it is highly unlikely that a feather will be subjected to this extreme damage during its lifetime, and one deformation cycle is a good measure.

Bending stiffness of the *rachis* is found to recover to a larger extent with a hydration step than without one, while the *calamus* recovers to a similar extent. This is likely due to the large difference in cross-sectional shape of the *rachis* with and without hydration after failure. The foam remains compressed after buckling in *rachis* samples without hydration, but swells and therefore recovers the original cross-sectional shape with hydration. The *calamus*, however, has a similar cross-sectional shape with and without hydration.

To describe the shape and strength recovery phenomena witnessed, a mechanism is proposed in which the hydrated matrix swells and has a lower flow stress than the fibers, which, in combination with fiber relaxation, results in the recovery of the shaft's shape and strength. Sections of the feather shaft were experimentally found to swell when hydrated, with the *rachis* swelling more extremely in circumference than the *calamus*, and the *calamus* swelling to a greater extent in the length. These results support the hypothesized behavior of the matrix and demonstrate that swelling occurs predominantly in the direction perpendicular to the fibers. Last, a section of the cortex was simulated in bending with a hydration step, providing insight into the recovery of the shape.

The strength recovery of the feather with hydration might contribute to an explanation for why birds of most species take baths. In a behavioral biology study, it was found that birds with access to bathing water flew more accurately than those without bathing water.<sup>[23]</sup> Our research here serves as a possible explanation for why bathing is highly important to the bird. Understanding the phenomenon witnessed with strength recovery in the feather shaft can be applied to further the capabilities of shape memory composites, resulting in new smart, self-healing materials.

### 4. Experimental Section

*Test Specimens:* Flight feathers of the Cape Vulture (*Gyps coprotheres*) were obtained postmortem and stored in ambient conditions. These feathers were used because they were large enough to conduct tensile tests on cortex material from each side of the feather to determine differing elastic moduli (Sections S.3 and S.4 in the Supporting Information). Sections of the *calamus* and *rachis* were sliced with a razor and measured using calipers to ensure similar dimensions between samples. The ends of each feather shaft section were then fixed in the center of a 5 mm square aluminum tube using epoxy to prepare samples for bending tests. Each completed sample had 18 mm of exposed *rachis* between the blocks, with a block length of 22 mm in length at each end. Cortex samples used in swelling and tension tests were sliced into rectangular pieces from each corresponding section of the *rachis* or *calamus*.

*Flexure Tests on the Feather Shaft:* *Calamus* and *rachis* samples were tested in four-point bending to mitigate the effects of the naturally curved feather shaft and prevent local crushing stresses. Bending tests were initially done directly on feather sections, but due to the nonuniform cross section of the shaft, samples rotated, and twisted in loading, preventing measurement of pure bending. To address this

issue, the method adapted was developed by Corning and Biewener<sup>[24]</sup> in which tests were conducted on the feather sample with its ends embedded (as described previously).

Feather samples were tested with their dorsal side facing upward, to mimic the main loading orientation on the feather shaft when the bird was in flight. As shown in Figure S.6 in the Supporting Information, steel rollers of the top and bottom fixtures were placed at the inner and outer most location of the blocks. A rate of displacement of 0.01 mm s<sup>-1</sup> was applied using an Instron Universal Testing Machine model 3347 (Instron Corporation, Norwood, MA, USA).

**Cyclical Flexure Tests on the Feather Shaft:** All 20 *calamus* and *rachis* samples were tested to failure for five cycles. Five of the *calamus* and *rachis* samples were hydrated for 24 h between stress cycles, while the other half were not. Samples were given the same amount of recovery time in total, with hydrated samples allowed to dry for 72 h in ambient conditions, and dry samples placed in ambient conditions for 96 h. Before and after tests, samples were imaged using optical microscopy. Additionally, each sample was weighed before testing. This ensured that hydrated samples had returned to their original state.

**Water Retention and Swelling Experiments:** The *rachis* and *calamus* were sliced into sections as well as rectangular cortex strips. Optical microscopic images and the initial mass of each sample were recorded before and after 24 h of hydration. Dimensions were measured using ImageJ software (National Institutes of Health, Bethesda, MD).

**Shape Recovery Composite:** The shape memory composite was fabricated from layers of cellulose sponge material with a stiffer steel wool top (dark “fibers” in Figure 2c) adhered in layers with drops of a cyanoacrylate adhesive. The cellulose sponge and steel wool fibers were chosen because of the dramatic contrast between their ability to swell with hydration. The cellulose sponge swells a considerable amount with hydration, while the steel wool fibers do not noticeably swell. This difference provided the contrast required to easily visualize shape recovery of the layered composite. Optical microscopic images were taken before deformation, after deformation, and after hydration.

## Supporting Information

Supporting Information is available from the Wiley Online Library or from the author.

## Acknowledgements

The authors graciously thank Mason Mackey at the National Center for Microscopy and Imaging Research as well as Haocheng Quan and Dr. Shiteng Zhao for assistance with TEM. The authors also thank the Los Angeles Zoo (Mike Maxcy, Curator of Birds and Dr. Cathleen Cox, Director of Research) for providing feather samples to us. This work was part of the AFOSR MURI (AFS0R-FA9550-15-1-0009). Y.Z. and P.D.Z. would like to acknowledge partial support by the National Science Foundation through the GOALI award CMMI-1538898.

## Conflict of Interest

The authors declare no conflict of interest.

## Keywords

nanocomposites, self-healing, shape memory, strength recovery

Received: February 15, 2018

Revised: April 11, 2018

Published online: May 28, 2018

- [1] C. J. Pennycuik, *Modelling the Flying Bird*, 1st ed., Elsevier, Burlington, USA **2008**.
- [2] F. B. Gill, *Ornithology*, 2nd ed., W. H. Freeman, New York, USA **1995**.
- [3] B. Wang, W. Yang, J. McKittrick, M. A. Meyers, *Prog. Mater. Sci.* **2016**, *76*, 229.
- [4] B. Wang, M. A. Meyers, *Adv. Sci.* **2016**, *4*, 1600360.
- [5] T. Lingham-Soliar, R. H. C. Bonser, J. Wesley-Smith, *Proc. R. Soc. Edinburgh, Sect. B: Biol. Sci.* **2010**, *277*, 1161.
- [6] J. McKittrick, P. Y. Chen, S. G. Bodde, W. Yang, E. E. Novitskaya, M. A. Meyers, *JOM* **2012**, *64*, 449.
- [7] R. D. B. Fraser, T. P. MacRae, G. E. Rogers, *Keratins: Their Composition, Structure and Biosynthesis* (Ed: C. Thomas), **1972**.
- [8] C. M. Laurent, C. Palmer, R. P. Boardman, G. Dyke, R. B. Cook, *J. R. Soc., Interface* **2014**, *11*, 20140961.
- [9] M. Feughelman, *Mechanical Properties and Structure of Alpha-Keratin Fibers: Wool, Human Hair and Related Fibers*, University of New South Wales Press, Sydney, Australia **1997**.
- [10] R. D. B. Fraser, T. P. MacRae, in *Molecular Structure and Mechanical Properties of Keratins* (Eds: J. F. V. Vincent, J. D. Currey), Cambridge University Press, Cambridge, UK **1980**, pp. 211–246.
- [11] Z. Q. Liu, D. Jiao, Z. F. Zhang, *Biomaterials* **2015**, *65*, 13.
- [12] M. Feughelman, M. S. Robinson, *Text. Res. J.* **1967**, *37*, 441.
- [13] Z. Q. Liu, D. Jiao, M. A. Meyers, Z. F. Zhang, *Acta Biomater.* **2015**, *17*, 137.
- [14] X. Xiao, J. Hu, *Sci. Rep.* **2016**, *6*, 26393.
- [15] X. Xiao, J. Hu, X. Gui, J. Lu, H. Luo, *Polym. Chem.* **2017**, *8*, 283.
- [16] X. Xiao, J. Hu, X. Gui, K. Qian, *Polymers* **2017**, *9*, 87.
- [17] X. Xiao, H. Zhou, K. Qian, *Smart Mater. Struct.* **2017**, *26*, 035023.
- [18] Z. Q. Liu, D. Jiao, Z. Y. Weng, Z. F. Zhang, *J. Mech. Behav. Biomed. Mater.* **2016**, *56*, 14.
- [19] H. Meng, G. Li, *Polymer* **2013**, *54*, 2199.
- [20] W. M. Huang, B. Yang, Y. Zhao, Z. Ding, *J. Mater. Chem.* **2010**, *20*, 3367.
- [21] K. Oliver, A. Seddon, R. S. Trask, *J. Mater. Sci.* **2016**, *51*, 10663.
- [22] J. B. Speakman, *Trans. Faraday Soc.* **1929**, *25*, 92.
- [23] B. O. Brillot, L. Asher, M. Bateson, *Anim. Behav.* **2009**, *78*, 801.
- [24] W. Corning, A. Biewener, *J. Exp. Biol.* **1998**, *201*, 3057.
- [25] B. Wang, M. A. Meyers, *Acta Biomater.* **2017**, *48*, 270.